Journal of Taibah University Medical Sciences (2023) 18(6), 1200–1216

Taibah University

Journal of Taibah University Medical Sciences

www.sciencedirect.com

Original Article

Homology modeling, docking, and ADMET studies of benzoheterocyclic 4-aminoquinolines analogs as inhibitors of *Plasmodium falciparum*

Zakari Y. Ibrahim, MSc *, Adamu Uzairu, PhD, Gideon A. Shallangwa, PhD, Stephen E. Abechi, PhD and Sulaiman Isyaku, PhD

Department of Chemistry, Faculty of Physical Sciences, Ahmadu Bello University, Zaria, Nigeria

Received 3 January 2023; revised 18 February 2023; accepted 20 April 2023; Available online 2 May 2023

الملخص

أهداف البحث: يتم ضمان الكفاح المستمر ضد الأمراض المستوطنة من خلال مقاومة طفيل الملاريا المتزايدة للأدوية المتاحة على نطاق واسع. وهكذا، فإن البحث عن الأدوية المضادة للملاريا ذات الفعالية المحسنة يتحول إلى بحث دائم. يهدف البحث إلى تطوير مشتقات البنزوهيروسيكليك 4-أمينوكينولين مع أنشطة محسنة وارتباطات أفضل من المركبات الأصلية.

طريقة البحث: تم إرساء أربعة وثلاثون مشتقا من البنزوهيروسيكليك 4-أمينوكينولين باستخدام برنامج "موليقرو" لتحديد المركب مع الحد الأدنى من نقاط الإرساء كقالب تصميم. سيتم نشر نموذج العلاقة الكمية بين البنية والفعالية الناتج في تقدير نشاط المشتقات المصممة. تم أيضا تثبيت المشتقات لتحديد أكثر المشتقات تصميما ثباتا. علاوة على ذلك، تم اختبار المشتقات المصممة لتشابه الأدوية باستخدام برنامج "سويس أدمي" و تم تم اختبار خصائصها الحركية باستخدام تطبيق الويب "بي كيه سي اس ام".

النتائج: المركب "اتش-014" بأدنى درجة إعادة تصنيف تبلغ -115.423 كيلو كالوري/مول كقالب تصميم. من هذه المشتقات العشرة (10) تم تصميمها أيضا عن طريق استبدال مجموعات في مواضع مختلفة من القالب. وجدت الدراسة أن المشتقات المصممة لديها أنشطة محسنة عن النموذج. كانت درجات الالتحام لمشتقات التصميم أقل من تلك الخاصة بالمشتقات الأصلية. تم تحديد مشتق "اتش-06" بأربعة روابط هيدروجينية، الأكثر استقرارا نظرا لأدنى درجة إعادة تصنيف لها (-163.607 كيلو كالوري / مول). بينما تمر جميع المشتقات المصممة كلا من قواعد ليبينسكي وفيربر، فإن بعضها مثل المشتقات "اتش-010"، "اتش-05"، "اتش-08"، "اتش-09"، "اتش-03"، "اتش-07" تظهر خصائص ضعيفة لامتصاص وتوزيع وتمثيل الدواء وإفرازه.

الاستنتاجات: تم تصميم عشرة مشتقات من البنزوهيروسيكليك 4-أمينوكينولين بكفاءة محسنة. بعد الامتثال لقواعد ليبينسكي وفيربر وهي في الغالب غير سامة وغير حساسة للجلد، يمكن استخدام المشتقات في تطوير أدوية فعالة مضادة للملاريا.

الكلمات المفتاحية: نمذجة العلاقة الكمية بين البنية والفعالية؛ الالتحام؛ البنزوهيروسيكليك 4-أمينوكينولين

Abstract

Objectives: The ongoing fight against endemic diseases is necessary due to the growing resistance of malarial parasites to widely accessible medications. Thus, there has been an ongoing search for antimalarial medications with improved efficacy. The goal of this study was to develop derivatives of benzoheterocyclic 4-aminoquinolines with enhanced activities and better binding affinities than the original compounds.

Methods: Thirty-four derivatives of benzoheterocyclic 4-aminoquinolines were docked (using a model of dihydrofolate reductase-thymidylate synthase [DRTS] protein) with Molegro software to identify the compound with the minimum docking score as a design template. The generated quantitative structure–activity model was employed to estimate the activity of the designed derivatives. The derivatives were also docked to determine the most stable derivatives. Furthermore, the designed derivatives were tested for their drug-likeness and pharmacokinetic properties using SwissADME software and pkCSM web application, respectively.

Results: Compound H-014, (*N*-(7-chloroquinolin-4-yl)-2-(4-methylpiperazin-1-yl)-1,3-benzoxazol-5-amine) with the lowest re-rank score of −115.423 was employed as the

* Corresponding address: Department of Chemistry, Faculty of Physical Sciences, Ahmadu Bello University, Zaria, Nigeria.
E-mail: zakariyyadibrahim@gmail.com (Z.Y. Ibrahim)

Peer review under responsibility of Taibah University.

ELSEVIER Production and hosting by Elsevier

 https://doi.org/10.1016/j.jtumed.2023.04.005

design template. Then 10 derivatives were further designed by substituting −OH, $-OCH_3$, −CHO, −F, and -Cl groups at various positions of the template. We found that the designed derivatives had improved activities compared to the template. The docking scores of the designed derivatives were lower than those of the original derivatives. Derivative h-06 (7-methoxy-4-((2-(4-methylpiperazin-1-yl)benzo[d]oxazol-5-yl)amino)quinolin-6-ol) with four hydrogen bonds was identified as the most stable due to its lowest re-rank score (−163.607). While all of the designed derivatives satisfied both the Lipinski and Verber rules, some derivatives such as h-10 (cytochrome P450 1A2 [CYP1A2]); h-05, h-08, h-09, and h-10 [CYP2C19]; and h-03, h-07, h-08, and h-10 [renal organic cation transporter 2 substrate]) showed poor absorption, distribution, metabolism, excretion, and toxicity (ADMET) properties.

Conclusion: Ten derivatives of benzoheterocyclic 4-aminoquinolines were designed with improved efficacies. Derivatives that follow Lipinski and Verber rules and are mostly non-toxic and non-sensitive to the skin can be utilized in the development of effective antimalarial medications.

Keywords: Benzoheterocyclic 4-aminoquinolines; Docking; Homology modeling; QSAR

Introduction

Human malaria is a potentially fatal disease that spreads through the bite of infected female Anopheles mosquitoes. In 2022, there was an estimated 247 million malaria cases and a death toll of 619,000 globally.[1] The genus *Plasmodium*, existing in diverse species *Plasmodium falciparum*, *P. vivax*, *P. ovale*, *P. knowlesi*, and *P. malariae*, is responsible for malaria.

Most cases of malaria are caused by *P. vivax* and *P. falciparum* globally. Although *P. falciparum* causes more fatalities, *P. vivax* is the most common malaria species and can lead to serious, even deadly attacks, and has a considerable impact on morbidity and death rates worldwide.[2] Drugs such as quinine, pyrimethamine, proguanil, chloroquine, and mefloquine as well as artemisinin atovaquone have all been suggested for the treatment of malaria.[3–5] *Plasmodium* species have grown resistant to most of these widely prescribed medications.

In recent times, treating malaria has grown significantly more difficult because of this resilience and the absence of a vaccine.[6] Hence, there is an urgent need to identify new antimalarial compounds as well as to increase the effectiveness of compounds by altering them to combat the resistance of the administered drugs.

The appeal of computational techniques in the discovery and design of drugs has improved because of their consistency in identifying compounds with strong pharmacological characteristics. Quantitative structure−activity (QSAR) analysis and homology modeling have found applications in several fields of research.[7–9] The molecular docking technique is frequently used to evaluate the binding affinities of drug candidates[10–12] as well as determine the appropriate orientations of the drug molecules in the protein-active region. Furthermore, *in silico* drug-likeness and absorption, distribution, metabolism, excretion, and toxicity (ADMET) properties determinations virtually screen potential drug-like compounds with biological activity.

The goal of this research was to use structure-based design methods to create certain benzoheterocyclic 4-aminoquinolines analogs with enhanced target binding and greater activity. Then the designed derivatives were put through docking tests to determine their affinity for attacking the protein target, and their hypothetical activities were calculated from the developed activity model. The drug-likeness and ADMET attributes of the produced compounds will also be assessed.

Materials and Methods

Data source and molecular descriptors

To perform the modeling, the reported experimental activities of the novel benzoheterocyclic 4-aminoquinolines derivatives[13] in Table 1, were employed as the sovereign variable. The activities reported in half-maximal inhibitory concentration (IC_{50}, μM) were converted to pIC_{50} (negative logarithm to base 10 of the drug that will reduce the cell growth by 50%). Chemdraw software was used to sketch the geometries, which were optimized with Spartan 14 software according to the density functional theory level and Becke's three-parameter Lee-Yang-Parr hybrid functional in conjunction with the 6-31+G* basis set,[14] and were conserved in standard data entry form. Approximately 1600 descriptors were calculated using PaDEL software after the stored geometries were accessed.

Dataset pretreatment and partition

Descriptors with a constant value, high coefficients of correlation, and variance levels below 0.001 were all removed. The pretreated dataset was thereafter partitioned with the aid of Kennard-algorithm Stone's approach into 26 training sets and 8 test sets[15] for model validation.

Selection of variables and model generation

Two quantitative structure−activity relationship (QSAR) models, which served as bridges between experimental activities and computed chemical descriptors, were developed to evaluate the activities using Materials Studio Version 8.0. To generate a viable model, the search for workable combinations of molecular descriptors was assisted through the material studio using its genetic function algorithm component.[16] With the smoothing parameter fixed at 0.5 and the mutation probability set to 0.1, we were able to obtain the top two QSAR regression models. To evaluate the models, the coefficient of determination (R^2) and externally verified

R^2 (R^2pred) values[17] were used. The best model was chosen thanks to the strong R^2, Q^2, and R^2pred values.

QSAR model validation

The leave-one-out (LOO) cross-validation internal validation approach was employed to validate the produced model. The cross-validated R^2 (Q^2cv) coefficient was calculated using equation (1) after deleting a dataset, and a predictive model was built utilizing the training data that was left behind. Then the activity of the dataset intended for deletion was predicted using the newly formed model. Once the activities of the deleted data were established, these processes were repeated until each dataset was individually removed.

$$Q^2_{cv} = 1 - \left[\sum (G_i - \hat{G}_i)^2 \Big/ \sum (G_i - G_{mean})^2\right] \quad (1)$$

where G_i is the actual activity, $\hat{G}_i$ is the predicted activity of the ith molecule in the training set, and G_{mean} is the overall average activity of all molecules in the training set.[18] Estimation of the activities of the test set was achieved via external validation. Using this approach, the data were partitioned into training and test sets. While the training set was for generating the activity model, the activities of the test set were predicted with the developed model.

Y-randomization test analysis

Another consideration during the model-building process is the Y-randomization test. This analysis was conceived as external validation to determine if the developed model occurred by chance versus randomly shuffling the training data.[19] To generate the activity model, the biological activities (dependent variables) were shuffled while maintaining the descriptors (independent variables). Compared to models with fixed activities, predictions for scattered activities models should have lower R^2 and Q^2 values. Additionally, for the model to be considered robust, the Y-randomization coefficient (cR^2p) shown in equation (2) needs to be greater than 0.5.

$$cR^2_p = R\,X\left[R^2 - (R_r)^2\right]^2 \quad (2)$$

where R_r is the medium of 'R' of randomized models and R is the coefficient correlation.

Applicability domain

The applicability domain (AD), also known as the Williams plot of a QSAR model, defines the chemical space upon which compounds are found, since no model, no matter how reliable or tested, can filter all chemical compounds. It refers to how well a QSAR model can withstand the inclusion of additional chemicals.[20] Defined by the region under ±3 regularized residuals and the leverage with brink value represented as $z^* = 3(t + 1)/n$. With t as the count of the descriptors in the model and n, as the amount of training data. Equation (3) is deployed in estimating the leverages.[21]

$$H = \left(X^T (X^T X)^{-1} X\right) \quad (3)$$

where H is an $[m \times m]$ matrix that orthogonally projects vectors into the space spanned by the columns of X.[22]

Homology modeling

The K1 strain protein sequence for *P. falciparum,* dihydrofolate reductase-thymidylate synthase (DRTS) shown in Figure 1, was redeemed from Universal Protein Resource Knowledge base (UniProtKB) webserver, http://www.uniprot.org with accession code: P13922.[23] The accession code was copied and put into the online workspace SWISSMODEL (https://www.swissmodel.expasy.org) for validation. The Basic Local Alignment Search Tool (BLAST)[24] and a Hidden Markov model-based lightning-fast iterative sequence search (HHblits) were used to identifying viable templates.[25] Using the ProMod3 modeling engine, the top-ranked aligned template from the alignment findings was chosen to create a new, energy-minimized protein model.[26] The Qualitative Model Energy Analysis (QMEAN) and Global Model Quality Estimation (GMQE) scores[27,28] were used to evaluate the dependability of the modeled three-dimensional (3D) structure.

Preparation of ligand and protein target

From the SWISS-MODEL interface, the homology model of DRTS target protein (Protein Data Bank [PDB] file) was obtained.[26] The complex ligands were eliminated using Discovery Studio, and the modeled protein was taken into consideration as the receptor. The preparation wizard feature of the MVD was used to prepare the protein and the ligand structures within the grid resolution set at 0.30 Å and the binding site radius as 15 Å relative to the origin of the corresponding cavities. In addition, the Molegro Virtual Docker (MVD) software can identify cavities during the interactions between ligands and protein targets. The modes of interaction detection-based algorithm identified through the MVD cavity was used to finish the docking investigations, and the outcomes were communicated via scoring functions.

Docking protocol validation

The re-docking of the crystallized ligand into the protein receptor's binding region served to confirm the docking process. The docked posture was superimposed with the initial crystallized ligand to get the root mean square deviation value (RMSD). The docking techniques were validated and their use in docking was confirmed by the permissible range of the RMSD value within ≤2.0 Å.[29]

Designing derivatives

The structure-based drug design (direct approach) uses a 3D structure to create novel therapeutic compounds with improved activity. Therefore, the derivative with the minimum binding energy in addition to the greatest tendency to bind the target was selected as the design template. To create different derivatives of the template, the characteristics that cause the high binding energy were substituted at different locations on the template. The proposed derivatives were also docked to determine their aptitude for the model of the DRTS target, and their activities were predicted using the pre-existing model. We looked at the potential analogs' drug-likeness and pharmacokinetic characteristics.

Drug likeness and pharmacokinetic evaluations

The drug-likeness of the developed derivatives as a prospective drug was determined using SwissADME software using Lipinski's rule of five (Ro5), while their pharmacokinetic characteristics were assessed using the pkCSM web application.[30] To decrease the frequency of clinical testing and increase drug effectiveness, drug-likeness as well as pharmacokinetic features of the entire derivatives were predicted.

Result and discussions

Regression equations

To create the selected regression equations, the datasets were examined using the genetic function approach, and are displayed below:

$$N = 26, R^2 = 0.9584, R^2_{Adj} = 0.9480, Q^2cv = 0.9342, LOF = 0.1124, R^2_{ext} = 0.7085, N_{ext} = 8$$

$$pIC_{50} = -0.0870*(ATSC7s) + 1.3619*(maxssCH2) - 0.1096*(RNCS) - 0.0427*(RDF95u) + 0.3012(RDF75v) + 3.8082 \quad (B)$$

$$N = 26, R^2 = 0.9547, R^2_{Adj} = 0.9434, Q^2cv = 0.9277, LOF = 0.1223, R^2_{ext} = 0.6752, N_{ext} = 8$$

The high values of the R^2 and adjusted R^2_{adj} signify the robustness of the developed models. Although the models possessed the same number of descriptors, model A with the highest R^2 0.9584, R^2_{adj} 0.9480, Q^2cv 0.9342, and particularly, R^2_{ext} 0.7085 was selected as the best model. Table 2 provides definitions for the representative descriptors in the best model. A tiny residual value resulted from comparing

$$pIC_{50} = -0.0873*(\text{average centered Broto} - \text{Moreau autocorrelation} - \text{lag 7 [ATSC7s]}) + 1.3411*(\text{maximum atom} - \text{type E} - \text{State} - \text{CH2 [maxssCH2]}) - 0.1129*(\text{relative negative charge surface area [RNCS]}) + 0.2976*(\text{radial distribution function [RDF]75v}) - 0.0870*(\text{RDF95p}) + 3.8131 \quad (A)$$

Table 1: Benzoheterocyclic 4-aminoquinolines analogs with their activities against the K1 strain of *P. falciparum*.

S/N	PubChem ID	Structures	IC_{50} (μM)	pIC_{50}
H-1[a]	122185673	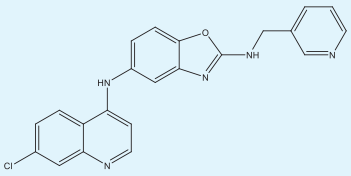	0.704	6.152
H-2	122185664	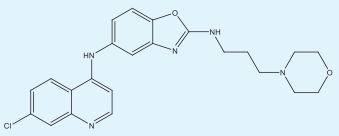	0.080	7.097
H-3	122185665	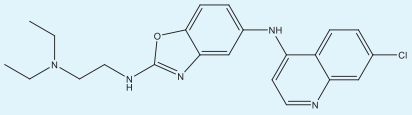	0.042	7.377
H-4[a]	122185666	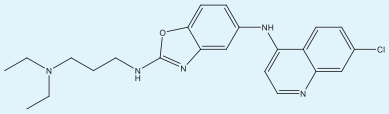	0.085	7.071

(*continued on next page*)

Table 1 (*continued*)

S/N	PubChem ID	Structures	IC_{50} (μM)	pIC_{50}
H-5	122185667	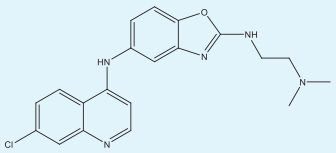	0.042	7.377
H-6	122185668	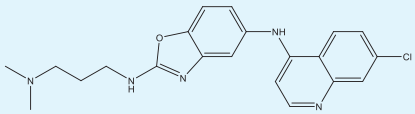	0.149	6.827
H-7	122185669	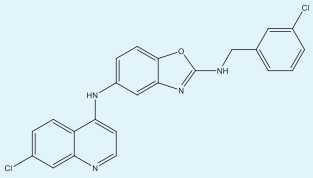	0.223	6.652
H-8	122185670	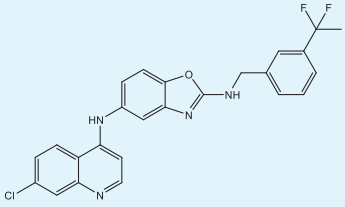	0.282	6.550
H-9	122185671	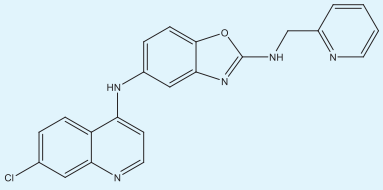	0.883	6.054
H-10	122185672	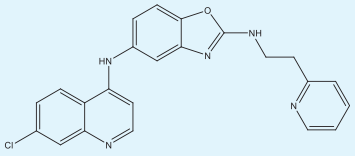	0.851	6.070
H-11[a]	122185674	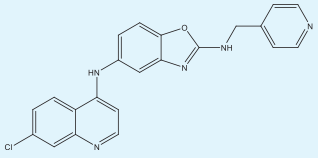	1.553	5.809
H-12	122185675	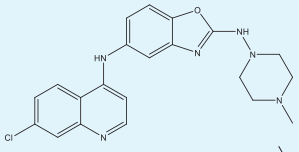	0.240	6.620
H-13[a]	122185676	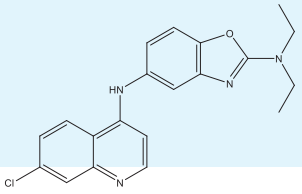	1.379	5.860

Table 1 (*continued*)

S/N	PubChem ID	Structures	IC_{50} (μM)	pIC_{50}
H-14	122185677	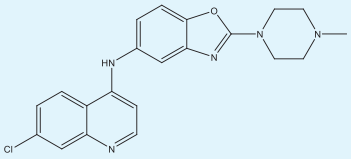	0.099	7.004
H-15	122185678	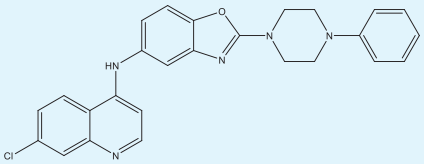	0.875	6.058
H-16	122185679	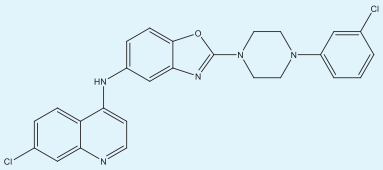	0.412	6.385
H-17	122185680	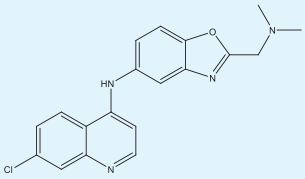	0.411	6.386
H-18	122185681	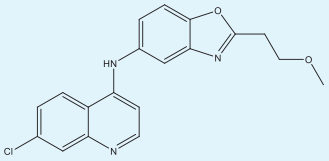	2.111	5.676
H-19	62706672	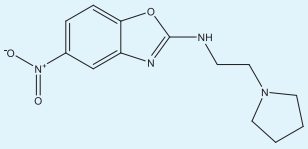	2.928	5.533
H-20[a]	122185662	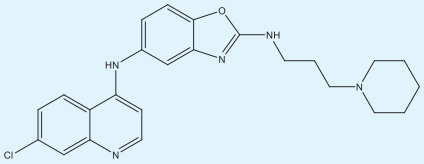	0.039	7.409
H-21[a]	62706335	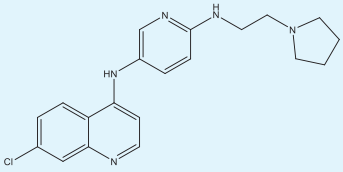	0.092	7.036
H-22	62706490	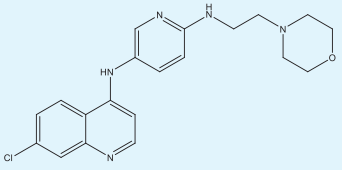	0.073	7.137

(*continued on next page*)

Table 1 (*continued*)

S/N	PubChem ID	Structures	IC_{50} (μM)	pIC_{50}
H-23	62706174	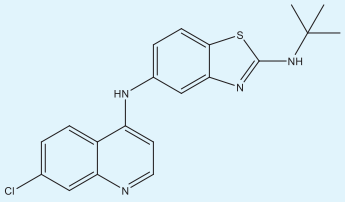	0.917	6.038
H-24	62706176	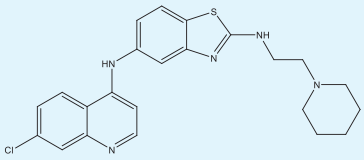	0.007	8.155
H-25[a]	62706177	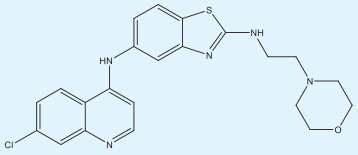	0.025	7.602
H-26	62706333	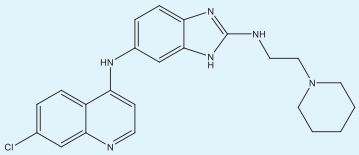	0.090	7.046
H-27	62706332	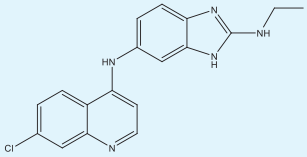	0.249	6.604
H-28	62706331	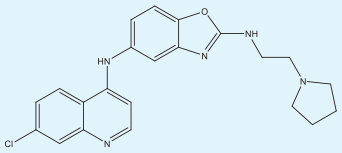	0.022	7.658
H-29	62706330	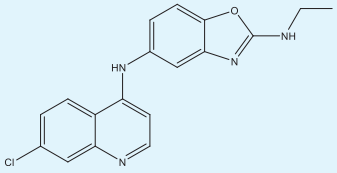	0.921	6.036
H-30[a]	122185659	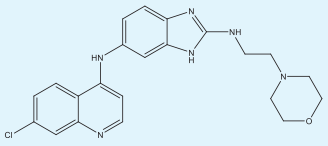	0.742	6.130
H-31	122185660	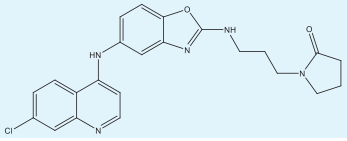	0.773	6.112

Table 1 (*continued*)

S/N	PubChem ID	Structures	IC_{50} (μM)	pIC_{50}
H-32	122185661	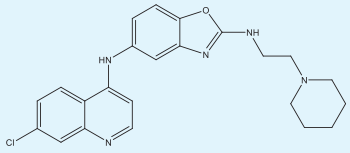	0.024	7.620
H-33	62706175	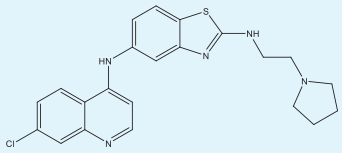	0.014	7.854
H-34	122185663	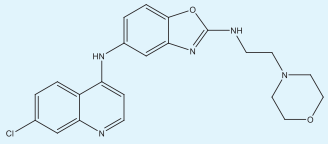	0.198	6.703
Chloroquine	2719	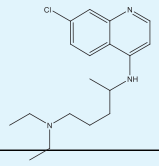	0.344	6.463

[a] Test set.

the anticipated to the actual activity of the models, as indicated in Figure 2, where the dataset was well distributed along the regression line.

Model validation

Through internal and external validation processes, the model's dependability was confirmed. The model quality and its robustness were guaranteed by the high results for Q^2_{cv} (0.9342) from the internal cross-validation procedure using LOO and R^2_{pred} (0.7085) from the test set. The correlation matrix analysis shown in Table 3, investigated the relationships between the model descriptors. Descriptors independent were shown via the low correlation coefficient, valued between −0.2485 and 0.5996 (<0.7).[31] Furthermore, the table revealed the contributory weights of the participating descriptors. Descriptor ATSC7s was shown to contribute 0.06778 (6.778%) to the generated model. Others were maxssCH2, which contributed 0.4350 (43.5%), and RNCS showed a negative weights contribution of −0.0769 (−7.69%), similar to descriptor RDF95p with −0.1337 (−13.37%) contribution. The most significant contributions come from descriptor RDF75v with 0.7079 consisting of 70.79% contribution.

Descriptors multicollinearity was also investigated through the variance inflation factors (VIFs) as reflected in Table 3. Here, the entire model descriptors were found to have VIF values less than 5, suggesting the orthogonality of the descriptors.[32] The Y-randomization test shown in Table 4 signifies the model's robustness. From the table, for randomized activity, the values of R^2 and Q^2 after 10-fold were lower than those for the unrandomized activity. In addition, the Y-randomization parameter (cR^2_p) was

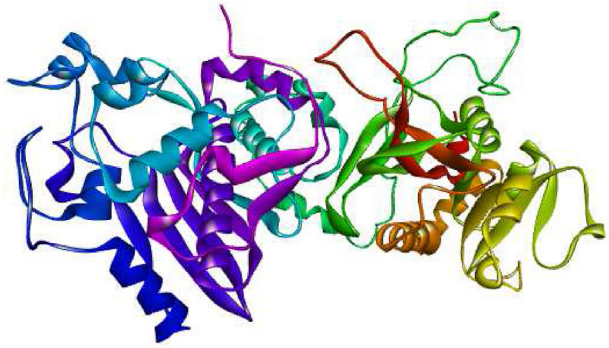

Figure 1: DRTS (PDB ID: 7f3Z.1A).

Table 2: Selected model's physiochemical descriptions.

S/N	Symbol	Names of descriptors	Class
1	ATSC7s	Centered Broto-Moreau autocorrelation - lag 7/weighted by I-state	2D
2	maxssCH2	Maximum atom-type E-State: −CH2-	2D
3	RNCS	Relative negative charge surface area − most negative surface area * RNCG	3D
4	RDF75v	Radial distribution function − 075/ weighted by relative van der Waals volumes	3D
5	RDF95p	Radial distribution function − 095/ weighted by relative polarizabilities	3D

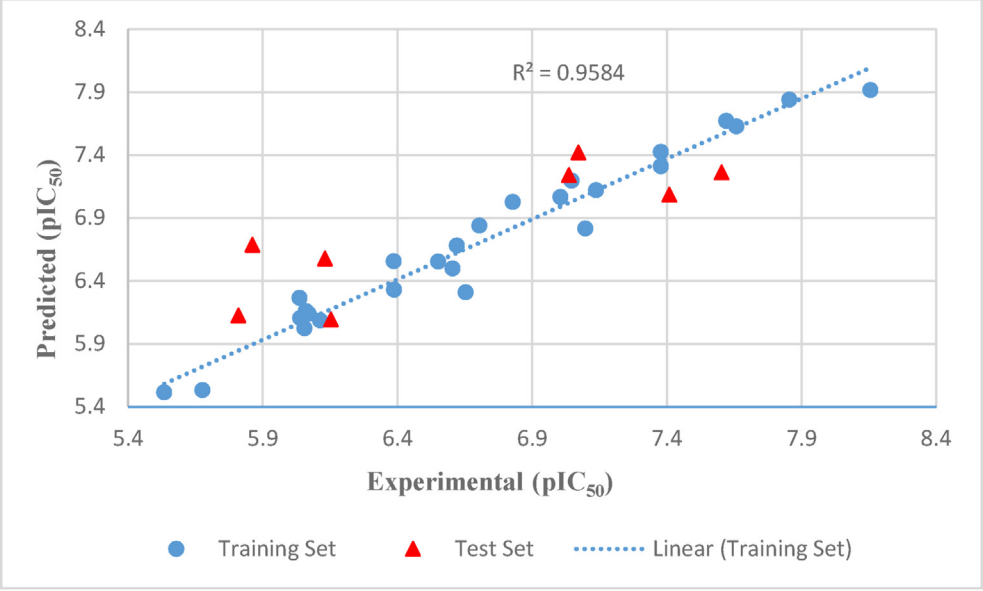

Figure 2: Dataset predicted pIC_{50} against the experimental values.

Table 3: Correlation matrix, mean effect, and the variation inflation factors of the regression equation.

	ATSC7s	maxssCH2	RNCS	RDF75v	RDF95p	VIF	Mean Effect
ATSC7s	1					1.0909	0.0678
maxssCH2	0.0991	1				1.7932	0.4350
RNCS	0.0612	−0.2485	1			1.0825	−0.0769
RDF75v	0.0611	0.0741	0.0384	1		1.1597	0.7079
RDF95p	−0.1123	0.5996	−0.1012	0.3155	1	1.8905	−0.1337

reported (Table 4) to be on the higher side of 0.5, further confirming the model.

Applicability domain (Williams plot)

The Williams plot, which compares the standardized residuals to the estimated leverage values, reveals the notable compounds and outliers in a model. The plots shown in Figure 3 were embedded within the 3 standardized residual ranges and a leverage threshold ($z^* = 0.69$). No compound was found beyond the leverage threshold of 0.69 and standardized residual of ±3.

Table 4: Parameters of Y-randomization models.

Model	R	R2	Q2
Original	0.9790	0.9584	0.9342
Random 1	0.5446	0.2966	−0.1379
Random 2	0.5105	0.2606	−0.1357
Random 3	0.6078	0.3694	−0.0413
Random 4	0.2423	0.0587	−0.5001
Random 5	0.2995	0.0897	−0.5870
Random 6	0.5783	0.3344	−0.0341
Random 7	0.6306	0.3976	−0.0876
Random 8	0.1383	0.0191	−0.7968
Random 9	0.5434	0.2953	−0.1569
Random 10	0.3905	0.1525	−0.7636
Random Models Parameters			
Average r:	0.4486		
Average r^2:	0.2274		
Average Q^2:	−0.3241		
cRp^2:	0.8519		

Homology modelling and structural validation

The Protein Data Bank database does not contain information about the dihydrofolate reductase-thymidylate synthase (DRTS) in *P. falciparum*. In order to find evolutionary related structures that matched the target sequence, the SWISS-MODEL template library was searched with the previously stated BLAST (near homologs) and HHBlits (distant homologs).[33] The search outcomes showed that the nearest template was the dihydrofolate reductase-thymidylate synthase (DRTS) structure of a functional obligatory respiratory super complex from *P. falciparum* (PDB: 7f3z.1A), which shared 80.56% identity and 90.6% query coverage with DRTS. Hence, the *P. falciparum* DRTS subunit homology model was constructed with a GMQE score of 0.87 and a QMEAN of 0.82, indicating high quality and dependability. The workspace produced local assessments of model quality using the QMEAN scoring function in relation to residue number and as a global score in reference to the high-resolution PDB structure set (Z score). To determine the local quality of the residues, a graph of the projected local similarity to target against the predicted number of residues in the model protein's anticipated 3D structure was plotted (Figure 4A). The majority of residue

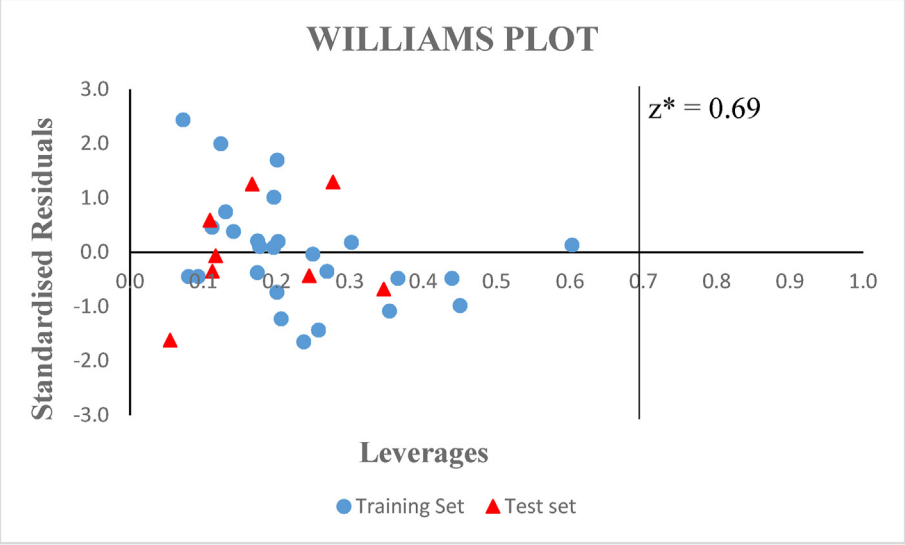

Figure 3: The plot of the standardized residuals versus the leverage values.

scores were found to be near to 1, indicating that the anticipated model has a reasonable local quality estimate. Residues with scores below 0.6 are considered to be of low quality. A plot of the normalized QMEAN score against the protein size was shown in Figure 4B, and it compares the model quality scores of individual models to estimates made for experimental structures of comparable sizes. When compared to the non-redundant set of PDB structures, the structure of the modeled protein was discovered to be within the acceptable range, demonstrating its dependability. Furthermore, both the Ramachandran plot (Figure 5) and its statistical parameters (Table 5) were obtained from procheck tool (https://saves.mbi.ucla.edu/) and are presented as a structure validation of the model of DRTS protein for stereochemical quality.

Molecular docking

To determine the ligands that bind to the model of DRTS protein most effectively, docking simulations were run on the whole dataset. The energies at which ligands bind to the model of DRTS protein are shown in Table 6 and are ranked based on their binding energies with novel benzoheterocyclic 4-aminoquinolines analogs. From the docking results, compound H-014 is shown to bind to the protein target better (by its minimum re-rank score, −115.423). Hence, it is used as a template (Figure 6) to develop further analogs with improved antimalarial activity and binding affinities.

Docking protocol validation

Assessment of the discrepancy between the re-docking output and the original docking position serves to identify and confirm the docking methods. The deviation shown in Figure 7 produces a RMSD value of 1.794 Å as its outcome. This demonstrates the effectiveness of the docking methods used to dock the designed template.

Designing derivatives

The examination of the complex, compound H-014-model of DRTS protein, reveals a variety of interactions

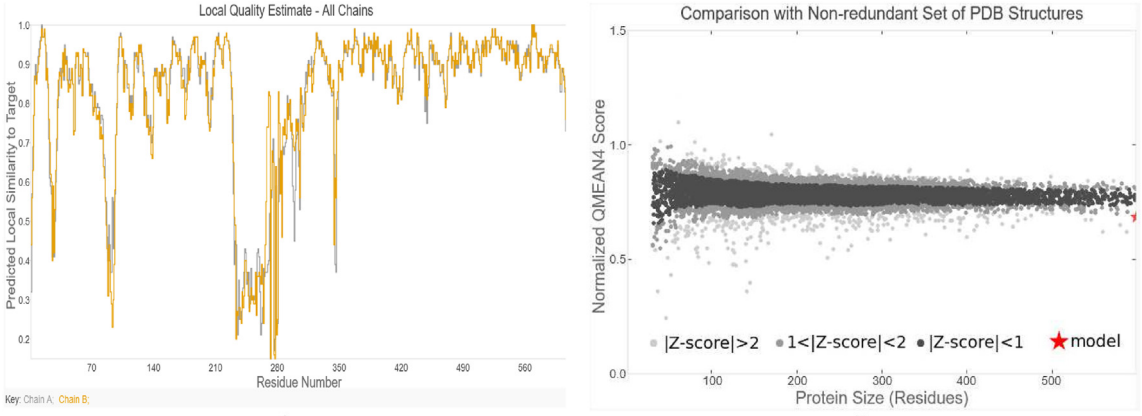

Figure 4: Structure validation of modeled *P. falciparum* DRTS protein structure: A: Local quality estimate of the residue graph. B: Comparison of the modeled protein structure with non-redundant set of PDB structures.

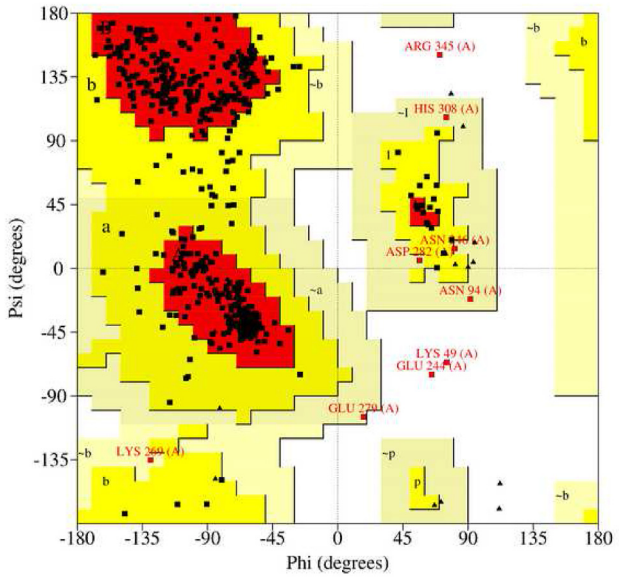

Figure 5: Ramachandran plot study of the DRTS from *P. falciparum*. While the color red denotes the favored zone, the color yellow denotes the allowed region, the color light yellow denotes the generously allowed region, and the color white denotes the banned region. Torsion angles are calculated using the Phi and Psi angles.

between the O, Cl, and F atoms of the model and the target. Ten analogs of the proposed design model shown in Table 7 were made by substituting −OH, $-OCH_3$, −CHO, −F, and -Cl groups at various points on the design model. It was discovered that the designed derivatives presented more challenging theoretical tasks than the template.

If the proposed derivatives cannot effectively limit the activities of their protein targets, their high binding affinities are useless. This necessitates the requirement to forecast the theoretical behaviors of the developed derivatives. This was accomplished with the use of the QSAR model developed earlier

Table 5: Ramachandran plot of DRTS from K1 strain of *P. falciparum*.

Ramachandran plot statistics	DRTS	
	Residue	%
Residues in most favored regions [A, B, L]	485	86.30
Residues in additional allowed regions [a, b, l, p]	68	12.1
Residues in generously allowed regions [∼a, ∼b, ∼l, ∼p]	6	1.1
Residues in disallowed regions	3	0.5
Number of non-glycine and non-proline residues	562	100.00
Number of end-residues (excl. Gly and Pro)	2	
Number of glycine residues (shown as triangles)	25	
Number of proline residues	19	
Total number of residues	608	

Table 6: MolDock score and re-rank score between the model of DRTS protein and the benzoheterocyclic 4-aminoquinolines analogs.

Ligand	MolDock Score	Re-rank Score
H-01	−121.066	−94.850
H-02	−162.656	−114.315
H-03	−114.643	−89.551
H-04	−84.075	−65.269
H-05	−135.158	−111.078
H-06	−99.168	−78.818
H-07	−89.034	−67.612
H-08	−102.403	−73.910
H-09	−103.398	−81.470
H-010	−106.035	−85.306
H-011	−99.370	−75.750
H-012	−131.107	−106.234
H-013	−117.449	−97.795
H-014	−141.091	−115.423
H-015	−125.392	−102.094
H-016	−137.006	−113.507
H-017	−110.351	−93.195
H-018	−120.885	−95.299
H-019	−113.462	−92.326
H-020	−93.396	−70.174
H-021	−116.859	−91.593
H-022	−126.993	−99.504
H-023	−115.098	−93.216
H-024	−140.599	−100.748
H-025	−127.952	−98.199
H-026	−96.712	−72.365
H-027	−130.757	−107.054
H-028	−120.115	−97.382
H-029	−115.221	−93.499
H-030	−113.973	−95.397
H-031	−103.707	−81.905
H-032	−133.363	−102.222
H-033	−122.337	−99.734
H-034	−105.451	−83.857
Chloroquine	−95.363	−78.325

(equation (4)), where it was discovered that their activities were superior to the template (7.004), as indicated in Table 7.

Furthermore, the theoretical activities of the designed derivatives, h-01, h-03, h-09, and h-10 were shown to be better than those of the parent derivatives. Then the designed derivatives were docked against the model of DRTS protein target as described earlier to ascertain their capacity to bind to the target. Because the designed counterparts had the lowest re-rank scores, docking assessments of the designed

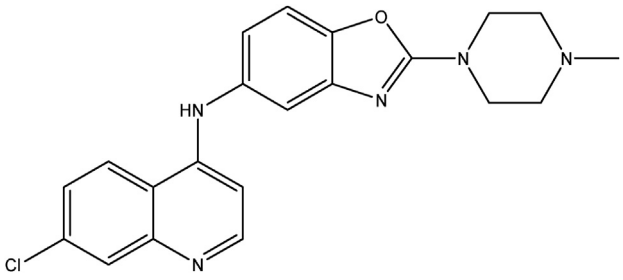

Figure 6: Template, Compound H-014, {*N*-(7-chloroquinolin-4-yl)-2-(4-methylpiperazin-1-yl)-1,3-benzoxazol-5-amine} re-rank score: −115.423 .

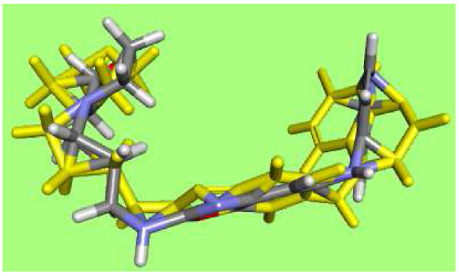

Figure 7: Superimposed image of the template compound after the re-dock.

Table 7: Template and designed derivatives of benzoheterocyclic 4-aminoquinolines inhibitors with their corresponding hypothetical activity.

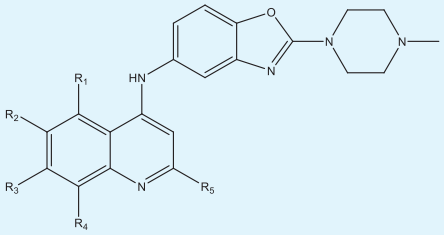

0S/N	R_1	R_2	R_3	R_4	R_5	Theoretical Activities	
						IC_{50} (μM)	pIC_{50}
Template	H	H	Cl	H	H	0.099	7.004
h-01	OH	H	Cl	OCH_3	H	0.00391	8.408
h-02	OH	OCH_3	Cl	H	H	0.01218	7.915
h-03	OH	OCH_3	CHO	H	H	0.00348	8.459
h-04	H	OCH_3	OCH_3	Cl	H	0.04367	7.360
h-05	H	F	OCH_3	H	H	0.02074	7.683
h-06	H	OH	OCH_3	H	H	0.08585	7.066
h-07	H	OH	F	H	H	0.06861	7.164
h-08	H	OCH_3	OCH_3	OH	Cl	0.09106	7.041
h-09	H	OCH_3	OH	OCH_3	Cl	0.00417	8.380
h-10	H	OCH_3	OH	OCH_3	F	0.00019	9.719

Table 8: MolDock score, re-rank score, and H-bond count between the model of DRTS protein and the designed derivatives of benzoheterocyclic 4-aminoquinolines analogs.

Ligand	MolDock Score	Rerank Score	H-bond count
h-01	−135.839	−117.378	1
h-02	−137.639	−124.015	2
h-03	−153.140	−135.200	2
h-04	−144.029	−124.307	0
h-05	−137.031	−117.468	0
h-06	−185.483	−163.607	4
h-07	−162.911	−146.223	0
h-08	−139.087	−121.835	1
h-09	−148.579	−123.077	0
h-10	−125.897	−110.936	0
Template	−141.091	−115.423	0
Chloroquine	−95.363	−78.325	0

analogs in Table 8 show that they had stronger binding attractions than the template and the standard. High binding attractions were made possible by the low binding energies between the suggested derivatives and the protein target. From the docking results (Table 8), designed derivative h-06 showed the lowest re-rank score (−163.607); hence, it was the most stable since it bound better to the target than the template and fellow designed derivatives. Designed derivative h-06 was possessed four hydrogen bonds. The molecular interactions shown in Table 9 provide the detailed interactions of the designed derivatives with the target protein. From the molecular interaction table, the four hydrogen bonds observed in derivative h-06 were each formed with Gly378, Ile379, Asn521, and Phe375 amino acid residues with 2.46 Å, 2.17 Å, 1.94 Å, and 1.85 Å respective bonds lengths. In addition to these, the derivative formed four carbon-hydrogen bonds with residues Gly378, two Ser511, and Asn521 with bond lengths 2.87 Å, 2.86 Å 2.43 Å, and 2.35 Å respectively. Derivative h-06 was also observed to undergo hydrophobic interactions forming three π-π stacked bonds each with residue Phe520 at bond lengths 5.15 Å, 4.33 Å, and 4.34 Å respectively. Other hydrophobic interactions observed by derivative h-06 are an alkyl bond with Cys490 (5.10 Å) and two π-alkyl bonds each with Ile403 (5.26 Å and 4.99 Å). The next stable derivative was h-07 with a re-rank score of −146.223, although it had no conventional hydrogen bonds, the low observed docking score could result from its various interactions with the protein target. Among the interactions were four carbon-hydrogen bonds with Ile112 (2.53 Å), two Pro113 (2.83 Å and 2.91 Å), and Gly166 (2.73 Å). Derivative h-07 reportedly had hydrophobic interactions such as three alkyls with amino residues Met55 (4.98 Å), Ile112 (4.32 Å), and Leu119 (5.47 Å). Other hydrophobic interactions of derivative h-07 were six π-alkyls with two Leu46s (4.85 Å and 3.88 Å), Ile112 (3.96 Å), Ile112 (5.26 Å), Leu40 (4.70 Å), and Val195 (4.51 Å) residues. The molecular interactions for the other generated derivatives of *N*-(7-chloroquinolin-4-yl)-2-(4-methylpiperazin-1-yl)-1,3-benzoxazol-5-amine are also shown in Table 9. The interactions between the most stable benzoheterocyclic 4-aminoquinolines derivatives are shown in Figure 8.

Predicted drug-likeness and pharmacokinetics of the designed derivatives

To forecast the drug-likeness of the proposed derivatives and how they would behave in human bodies, Lipinski's Ro5 and the Veber rule test were used. The Ro5 predicts the excellent bioavailability of drug molecules with less than 5 hydrogen bond donors, less than 10 hydrogen bond acceptors, molecular weight less than 500 Da, and a below 4.15 computed Mlog P. Table 10 displays the projected drug-likeness and pharmacokinetic outcomes for the developed derivatives. All of them were within the Ro5, thus passing Lipinski's test. Also, the designed derivatives followed the Veber rule, with their topological polar surface area (TPSA) all less than 140 $Å^2$ and nRotb values all below 10. Hence, in humans, the designed derivatives will be active orally.[34,35]

Table 9: Molecular interactions of the designed derivatives of benzoheterocyclic 4-aminoquinolines.

Inhibitor	Category	Type of interaction	Residues	Bond distance (Å)
h-01	Hydrogen Bond	Carbon Hydrogen Bond	His491 and two Tyr430	2.87,1.95, and 3.02
	Electrostatic	π-Anion	Glu382 and Glu382	4.26 and 4.32
	Hydrophobic	π−π stacked	Phe520	3.91
	Hydrophobic	alkyl	Leu487, and Cys490	4.83, 4.26
		π-alkyl	Trp404, Ile403, and Leu516	4.68, 4.54, and 5.27
h-02	Hydrophobic	π−π stacked	Two Phe375s and two Phe520's	3.81, 3.90, 4.58, and 3.68
		alkyl	Leu516	5.43
		π-alkyl	Two Ile403's, Phe520, and Ile379	4.75, 5.41, 4.86, and 5.18
h-03	Hydrogen Bond	Carbon Hydrogen Bond	His491 and two Phe375s	2.45, 2.29, and 2.69
	Electrostatic	π-anion	Glu382s	3.69 and 4.20
	Hydrophobic	π-π stacked	Trp404 and two Phe520s	5.62, 4.14, and 4.11
		π-alkyl	Phe375, Ile379, and three Ile403s	5.37, 5.47, 4.87, 4.15, and 5.16
h-04	Electrostatic	π-cation	Arg377	3.51
	Hydrophobic	π−π Stacked	Two Phe375s and Two Phe520s	4.67, 3.90, 4.62, and 3.61
		alkyl	Ile403	5.03
		π-alkyl	Two Ile379s, Ile403, Phe520, and Arg377	5.03, 5.30, 4.67, 4.63, and 4.79
h-05	Hydrogen Bond	Carbon Hydrogen Bond	Two Tyr430s	2.37 and 2.71
	Electrostatic	π-anion	Glu382	4.37
	Hydrophobic	π−π stacked	Two Phe520s	4.06 and 4.31
		alkyl	Cys490	4.75
		π-alkyl	Three Ile403s, Trp404, and Ile379	4.70, 4.10, 5.07, 4.63, and 5.00
h-06	Hydrogen Bond	Conventional Hydrogen Bond	Gly378, Ile379, Asn521, and Phe375	2.46, 2.17, 1.94, and 1.85
		Carbon Hydrogen Bond	Gly378, Two Ser511s, and Asn521	2.87, 2.86 2.43, and 2.35
	Hydrophobic	π−π stacked	Three Phe520s	5.15, 4.33, and 4.34
		alkyl	Cys490	5.10
		π-alkyl	Two Ile403s	5.26 and 4.99
h-07	Hydrogen Bond	Carbon Hydrogen Bond	Ile112, two Pro113s, and Gly166	2.53, 2.83, 2.91, and 2.73
		alkyl	Met55, Ile112, and Leu119	4.98, 4.32, and 5.47
		π-alkyl	Leu46, Ile112, Leu46, Ile112, Leu40, and Val195	4.85, 3.96, 3.88, 5.26, 4.70, and 4.51
h-08	Hydrogen Bond	Conventional Hydrogen Bond	Lys49	2.69
		Carbon Hydrogen Bond	Ile164	2.07
	Other	π-Sulfur	Met55	5.70
	Hydrophobic	alkyl	Ile112 and Pro113	4.59 and 4.52
		π-alkyl	Leu46, Phe58, Ile112, Pro113, Val45, Leu46, Pro113, Lys49, Pro113, and Lys49	3.89, 5.48, 5.10 5.27, 5.20, 4.23, 4.63, 5.26, 4.61, and 4.60
h-09	Hydrogen Bond	Carbon Hydrogen Bond	His491, Pro488, and three Tyr430s	2.73, 2.31, 2.11, 2.05, and 2.99
	Electrostatic	π-anion	Two Glu382s	4.08 and 4.18
	Hydrophobic	π−π stacked	Two Phe520s	3.99 and 3.72
		alkyl	Leu487, Cys490, and Leu516	4.86, 4.30, and 3.59
		π-alkyl	Ile403, Trp404, Tyr430, and two Ile403s	5.50, 4.64, 5.49, 4.58, and 5.40
h-10	Hydrogen Bond	Carbon Hydrogen Bond	Tyr274, Lys72, and Lys273	3.01, 2.74, and 2.82
	Electrostatic	π-cation	Two Lys275s	4.89 and 4.90
	Hydrophobic	π−π stacked	Two Tyrs274	3.87 and 4.61
		alkyl	Lys72 and Lys76	4.53 and 4.80
		π-alkyl	Lys275	4.57

ADMET evaluation

Poor ADMET properties are usually one of the main causes of drug failure.[36] Table 11 displays the theoretical ADMET characteristics of the developed derivatives. P-glycoprotein (P-gp) and human intestinal absorption were employed to evaluate the intake potentials of the designed derivatives. The human stomach has good absorption when the score is greater than 30%.[37] The designed derivatives were predicted to have exceptional human intestinal absorption where the designed derivatives scored higher than 80% as indicated in Table 11. One of the three mechanisms by which medications enter the cell is via P-gp, a major influence on the intake, redistribution, and elimination of a variety of drugs. P-gp can attach to a diverse range of substances found all over the body, and are found in crucial organs such as the kidney and liver as they are found in the small intestine.[38,39] All of the produced compounds were found to be P-gp substrates (Table 11). The blood−brain barrier (BBB) is used to

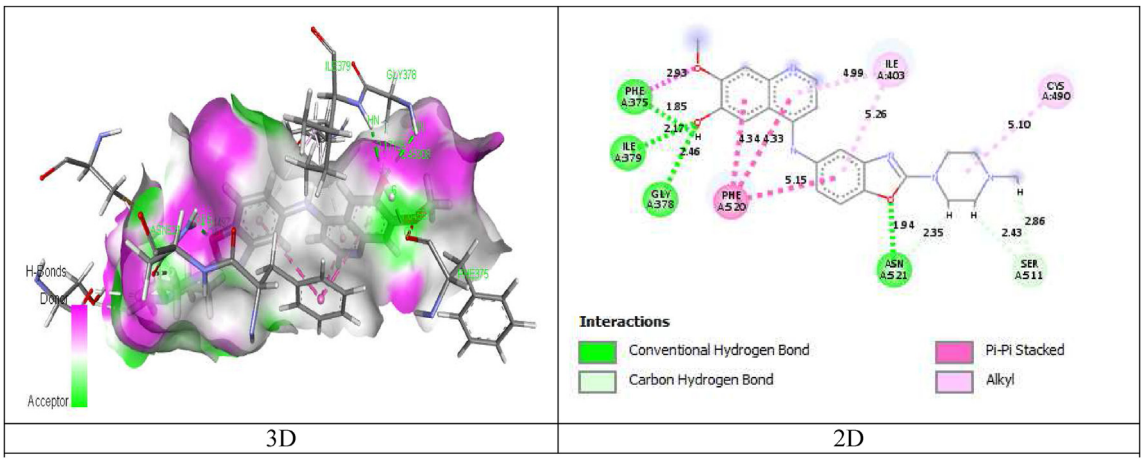

Figure 8: The most stable chemical, h-06, interacts with the model of DRTS protein in both 3D and 2D docking.

Table 10: Lipinski and Veber features for the designed benzoheterocyclic 4-aminoquinolines derivatives.

S/N	Lipinski's parameters					Veber parameters	
	MW (≤500Da)	MLOGP (<4.15)	#H-bond acceptors (≤10)	#H-bond donors (≤5)	Lipinski #violations	TPSA (<140 Å2)	nRotb (≤10)
h-01	439.89	2.04	6	2	0	86.89	4
h-02	439.89	2.04	6	2	0	86.89	4
h-03	433.46	0.93	7	2	0	103.96	5
h-04	453.92	2.25	6	1	0	75.89	5
h-05	407.44	2.46	6	1	0	66.66	4
h-06	405.45	1.56	6	2	0	86.89	4
h-07	393.41	2.24	6	2	0	77.66	3
h-08	469.92	1.74	7	2	0	96.12	5
h-09	469.92	1.74	7	2	0	96.12	5
h-10	453.47	1.64	8	2	0	96.12	5

Table 11: ADMET properties of the designed benzoheterocyclic 4-aminoquinolines derivatives.

S/N	Absorption		Distribution		Metabolism		Excretion		Toxicity	
	Intestinal absorption	P-gp substrate	BBB permeability	CNS permeability	CYP1A2 Inhibitor	CYP2C19 Inhibitor	Renal OCT2 substrate	Total Clearance	Skin Sensitivity	Oral Rat Acute Toxicity (LD_{50})
	Numeric (% absorbed)	Categorical (Yes/No)	Numeric (log BB)	Numeric (log PS)	Categorical (Yes/No)	Categorical (Yes/No)	Categorical (Yes/No)	(ml/min/kg)	Categorical (Yes/No)	mol/kg
h-01	91.038	Yes	−1.312	−2.305	Yes	Yes	Yes	0.699	No	2.935
h-02	91.330	Yes	−1.248	−2.299	Yes	Yes	Yes	0.769	No	3.073
h-03	85.355	Yes	−1.182	−2.67	Yes	Yes	No	0.951	No	2.894
h-04	93.740	Yes	−0.632	−2.292	Yes	Yes	Yes	0.681	No	3.216
h-05	94.214	Yes	0.070	−2.233	Yes	No	Yes	0.783	No	3.349
h-06	93.645	Yes	−1.135	−2.341	Yes	Yes	Yes	0.874	No	3.118
h-07	91.571	Yes	−1.095	−2.203	Yes	Yes	No	0.751	No	2.736
h-08	87.411	Yes	−1.387	−2.507	Yes	No	No	0.644	No	2.664
h-09	87.247	Yes	−1.253	−2.508	Yes	No	Yes	0.620	No	2.650
h-10	80.250	Yes	−1.232	−3.706	No	No	No	0.679	No	2.420

gauge how well a drug can pass across it without causing unwanted side effects. The BBB can be quickly crossed by a drug when the log BB is more than 0.3. Since the log BB values of all produced derivatives are less than 0.3, they can only just barely cross the BBB.[40,41] Additionally, typical the logarithm of the permeability-surface area coefficient (log PS) levels control a drug's central nervous system (CNS) accessibility. The drug is classified as CNS impenetrable within the $-3 > \log PS > -2$ range.[42] The designed derivatives all had log PS values less than −2, pointing to

their potential permeability. Enzyme metabolism demonstrates the transformation of drugs within the human system and is a dependable predictor of a drug's misuse potential. CYP450, especially CYP1A2 and CYP2C19, facilitates drug biotransformation.[43] All derivatives (except derivative h-10 for CYP1A2; derivatives h-05, h-08, h-09, and h-10) were found to inhibit CYP1A2 and CYP2C19, respectively, as shown in Table 11.

The overall clearance as well as the organic cation transporter 2 (OCT2) substrate excretion parameters are displayed in Table 11. Clearance is a unit used to quantify how quickly medicines leave the body relative to internal concentrations.[42] The capacity of the kidney to absorb, digest, and excrete drug molecules depends on the OCT2 protein transporter. There is an inverse correlation between renal OCT2 and overall clearance. Derivatives show high total clearance as indicated in Table 11. Furthermore, except for derivatives h-03, h-07, h-08, and h-10, all other derivatives showed renal OCT2 substrate potentials. Skin sensitivity tests as well as oral rat acute toxicity median lethal dose (LD_{50}) results were used to assess the theoretical toxicity of the developed compounds. While Table 11 shows that the oral rat acute toxicity LD_{50} values of the derivatives were within the 2.420−3.349 mol/kg range, it also indicates the insensitivity of the designed derivatives to the skin.

Conclusion

Thirty-four derivatives of benzoheterocyclic 4-aminoquinolines were employed in the design of ten improved derivatives using a structure-based technique. The designed derivatives demonstrated enhanced activity and had better scores when docked against a model of DRTS protein. Derivative h-06 (7-methoxy-4-((2-(4-methylpiperazin-1-yl)benzo[d]oxazol-5-yl)amino)quinolin-6-ol) with four hydrogen bonds was identified as the most stable due to its lowest re-rank score, −163.607. The four hydrogen bonds observed were formed each with Gly378, Ile379, Asn521, and Phe375 amino acid residues with bond lengths of 2.46 Å, 2.17 Å, 1.94 Å, and 1.85 Å, respectively. These and other interactions could be responsible for the high binding affinity of the derivative h-06. Although all of the developed derivatives satisfied the Lipinski and Verber guidelines, several of them, including derivatives h-10 (CYP1A2), h-05, h-08, h-09, and h-10 (CYP2C19), and h-03, h-07, h-08, and h-10 (renal OCT2 substrate), had subpar ADMET qualities. The derivatives can be used in the creation of potent antimalarial drugs since they complied with the Lipinski and Verber requirements and are typically non-toxic and non-skin-sensitive.

Source of funding

This research did not receive any specific grant from funding agencies in the public, commercial, or not-for-profit sectors.

Conflict of interest

The authors have no conflicts of interest to declare.

Ethical approval

This research does not require ethical approval.

Consent

On behave of the authors, I hereby granted the right of this entire article content to this journal.

Authors' contributions

ZYI conducted research, provided research materials, and organized and analyzed the data; AU, project administration, supervised the research, and provided logistic support; GAS, supervised the research, and provide the methodology; SEA, supervised the research and provides the software; SI, provide the software and performs the data curation. All authors have critically reviewed and approved the final draft and are responsible for the content and similarity index of the manuscript.

Availability of data

The datasets used for analysis during these studies were included in this published study.

References

1. World Health Organization. *World Malaria Report*; 2022. https://www.who.int/teams/global-malaria-programme/reports/world-malaria-report-2022. [Accessed 2 May 2023].
2. Menkin-smith L, Winders WT. *Plasmodium vivax, malaria parasite*. Published online 2022;1−8. https://www.britannica.com/print/article/359534.
3. Sennari G, Saito R, Hirose T, et al. Antimalarial troponoids, puberulic acid and viticolins; Divergent synthesis and structure-activity relationship studies. **Sci Rep 2017**; 7(1): 5−9. https://doi.org/10.1038/s41598-017-07718-3.
4. Jozefowicz-Korczynska M, Pajor A, Lucas Grzelczyk W. The ototoxicity of antimalarial drugs—a state of the art review. **Front Neurol 2021**; 12. https://doi.org/10.3389/fneur.2021.661740.
5. Belete TM. Recent progress in the development of new antimalarial drugs with novel targets. **Drug Des Dev Ther 2020**; 14: 3875−3889. https://doi.org/10.2147/DDDT.S265602.
6. Sondo P, Derra K, Lefevre T, et al. Genetically diverse Plasmodium falciparum infections, within-host competition and symptomatic malaria in humans. **Sci Rep 2019**; 9(1): 127. https://doi.org/10.1038/s41598-018-36493-y.
7. Mahapatra M, Mekap SK, Mal S, Sahoo J, Sahoo SK, Paidesetty SK. Coumaryl-sulfonamide moiety: unraveling their synthetic strategy and specificity toward h CA IX/XII, facilitating anticancer drug development. **Arch Pharm (Weinheim) 2023**. https://doi.org/10.1002/ardp.202200508. Published online January.
8. Abdullahi M, Adeniji SE, Arthur DE, Musa S. Quantitative structure-activity relationship (QSAR) modelling study of some novel carboxamide series as new anti-tubercular agents. **Bull Natl Res Cent 2020**; 44(1): 136. https://doi.org/10.1186/s42269-020-00389-7.
9. Swain SS, Paidesetty SK, Padhy RN. Development of antibacterial conjugates using sulfamethoxazole with monocyclic terpenes: a systematic medicinal chemistry based computational approach. **Comput Methods Progr Biomed 2017**; 140: 185−194. https://doi.org/10.1016/j.cmpb.2016.12.013.

10. Deghady AM, Hussein RK, Alhamzani AG, Mera A. Density functional theory and molecular docking investigations of the chemical and antibacterial activities for 1-(4-Hydroxyphenyl)-3-phenylprop-2-en-1-one. **Molecules 2021**; 26(12): 3631. https://doi.org/10.3390/molecules26123631.
11. Wang F-F, Yang W, Shi Y-H, Le G-W. Molecular determinants of thyroid hormone receptor selectivity in a series of phosphonic acid derivatives: 3D-QSAR analysis and molecular docking. **Chem Biol Interact 2015**; 240: 324–335. https://doi.org/10.1016/j.cbi.2015.09.008.
12. Liu S, Li Y, Wei W, Wang K, Wang L, Wang J. Design, synthesis, molecular docking studies and anti-HBV activity of phenylpropanoid derivatives. **Chem Biol Interact 2016**; 251: 1–9. https://doi.org/10.1016/j.cbi.2016.03.011.
13. Ongarora DSB, Strydom N, Wicht K, et al. Antimalarial benzoheterocyclic 4-aminoquinolines: structure–activity relationship, in vivo evaluation, mechanistic and bioactivation studies. **Bioorg Med Chem 2015**; 23(17): 5419–5432. https://doi.org/10.1016/j.bmc.2015.07.051.
14. Ibrahim ZY, Uzairu A, Shallangwa GA. Application of QSAR method in the design of enhanced antimalarial derivatives of azetidine-2-carbonitriles , their molecular docking. **Drug-likeness, and SwissADME Properties 2021**; 20(November 2020): 254–270. https://doi.org/10.22037/ijpr.2021.114536.14901.
15. Rajer-Kanduč K, Zupan J, Majcen N. Separation of data on the training and test set for modelling: a case study for modelling of five colour properties of a white pigment. **Chemometr Intell Lab Syst 2003**; 65(2): 221–229. https://doi.org/10.1016/S0169-7439(02)00110-7.
16. Oluwaseye A, Uzairu A, Shallangwa GA, Abechi SE. QSAR studies on derivatives of QUINAZOLINE-4(3H)-ONES with anticonvulsant activities. **J Eng Exact Sci 2018**; 4(2): 255–264. https://doi.org/10.18540/jcecvl4iss2pp0255-0264.
17. Golbraikh A, Tropsha A. Beware of q2. **J Mol Graph Model 2002**; 20(4): 269–276. https://doi.org/10.1016/S1093-3263(01)00123-1.
18. Schüürmann G, Ebert R-U, Chen J, Wang B, Kühne R. External validation and prediction employing the predictive squared correlation coefficient — test set activity mean vs training set activity mean. **J Chem Inf Model 2008**; 48(11): 2140–2145. https://doi.org/10.1021/ci800253u.
19. Hasanin T, Khoshgoftaar TM, Leevy JL, Seliya N. Examining characteristics of predictive models with imbalanced big data. **J Big Data 2019**; 6(1): 69. https://doi.org/10.1186/s40537-019-0231-2.
20. Ruiz IL, Gómez-Nieto MÁ. Study of the applicability domain of the QSAR classification models by means of the rivality and modelability indexes. **Molecules 2018**; 23(11): 2756. https://doi.org/10.3390/molecules23112756.
21. Minovski N, Župerl Š, Drgan V, Novič M. Assessment of applicability domain for multivariate counter-propagation artificial neural network predictive models by minimum Euclidean distance space analysis: a case study. **Anal Chim Acta 2013**; 759: 28–42. https://doi.org/10.1016/j.aca.2012.11.002.
22. Gadaleta D, Mangiatordi GF, Catto M, Carotti A, Nicolotti O. Applicability domain for QSAR models. **Int J Quant Struct Relationships 2016**; 1(1): 45–63. https://doi.org/10.4018/IJQSPR.2016010102.
23. McKie JH. Homology modelling of the dihydrofolate reductase-thymidylate synthase bifunctional enzyme of Leishmania major, a potential target for rational drug design in leishmaniasis. **Drug Des Discov 1994**; 11(4): 269–288. http://www.ncbi.nlm.nih.gov/pubmed/7727680.
24. Camacho C, Coulouris G, Avagyan V, et al. BLAST+: architecture and applications. **BMC Bioinf 2009**; 10(1): 421. https://doi.org/10.1186/1471-2105-10-421.
25. Remmert M, Biegert A, Hauser A, Söding J. HHblits: lightning-fast iterative protein sequence searching by HMM-HMM alignment. **Nat Methods 2012**; 9(2): 173–175. https://doi.org/10.1038/nmeth.1818.
26. Waterhouse A, Bertoni M, Bienert S, et al. SWISS-MODEL: homology modelling of protein structures and complexes. **Nucleic Acids Res 2018**; 46(W1): W296–W303. https://doi.org/10.1093/nar/gky427.
27. Shaik NA, Hakeem KR, Banaganapalli B, Elango R, editors. **Essentials of bioinformatics**, ume II. Springer International Publishing; 2019. https://doi.org/10.1007/978-3-030-18375-2.
28. Benkert P, Biasini M, Schwede T. Toward the estimation of the absolute quality of individual protein structure models. **Bioinformatics 2011**; 27(3): 343–350. https://doi.org/10.1093/bioinformatics/btq662.
29. Kontoyianni M, McClellan LM, Sokol GS. Evaluation of docking performance: comparative data on docking algorithms. **J Med Chem 2004**; 47(3): 558–565. https://doi.org/10.1021/jm0302997.
30. Martinez-Mayorga K, Madariaga-Mazon A, Medina-Franco JL, Maggiora G. The impact of chemoinformatics on drug discovery in the pharmaceutical industry. **Expet Opin Drug Discov 2020**; 15(3): 293–306. https://doi.org/10.1080/17460441.2020.1696307.
31. N'Dri JS, Koné MG-R, Kodjo CG, et al. Quantitative activity structure relationship (QSAR) of a series of azetidinones derived from dapsone by the method of density functional theory (DFT). ISSN 2455-4499 **IRA Int J Appl Sci 2017**; 8(2): 55. https://doi.org/10.21013/jas.v8.n2.p2.
32. Kim JH. Multicollinearity and misleading statistical results. **Korean J Anesthesiol 2019**; 72(6): 558–569. https://doi.org/10.4097/kja.19087.
33. Steinegger M, Meier M, Mirdita M, Vöhringer H, Haunsberger SJ, Söding J. HH-suite3 for fast remote homology detection and deep protein annotation. **BMC Bioinf 2019**; 20(1): 473. https://doi.org/10.1186/s12859-019-3019-7.
34. Lipinski CA, Lombardo F, Dominy BW, Feeney PJ. Experimental and computational approaches to estimate solubility and permeability in drug discovery and development settings 1PII of original article: S0169-409X(96)00423-1. The article was originally published in Advanced Drug Delivery Reviews 23 (1997). **Adv Drug Deliv Rev 2001**; 46(1–3): 3–26. https://doi.org/10.1016/S0169-409X(00)00129-0.
35. Veber DF, Johnson SR, Cheng HY, Smith BR, Ward KW, Kopple KD. Molecular properties that influence the oral bioavailability of drug candidates. **J Med Chem 2002**; 45(12): 2615–2623. https://doi.org/10.1021/jm020017n.
36. Ya'u Ibrahim Z, Uzairu A, Shallangwa GA, Abechi SE, Isyaku S. Quantitative Structure-Activity Relationship, Structure-based Design, and ADMET studies of pyrimethamine and cycloguanil analogs inhibitors of Plasmodium falciparum dihydrofolate reductase-thymidylate synthase (PfDHFR-TS). **Chem Phys Impact 2022**; 5:100132. https://doi.org/10.1016/j.chphi.2022.100132.
37. Zafar F, Gupta A, Thangavel K, et al. Physico1chemical and pharmacokinetic analysis of anacardic acid derivatives. **ACS Omega 2020**; 5(11): 6021–6030. https://doi.org/10.1021/acsomega.9b04398.
38. Ahmed II Juvale, Abdul Hamid AA, Abd Halim KB, Che Has AT. P-glycoprotein: new insights into structure, physiological function, regulation and alterations in disease. **Heliyon 2022**; 8(6):e09777. https://doi.org/10.1016/j.heliyon.2022.e09777.
39. Bors L, Erdő F. Overcoming the blood–brain barrier. Challenges and tricks for CNS drug delivery. **Sci Pharm 2019**; 87(1): 6. https://doi.org/10.3390/scipharm87010006.
40. Pratama MRF, Poerwono H, Siswodiharjo S. ADMET properties of novel 5-O-benzoylpinostrobin derivatives. **J Basic Clin Physiol Pharmacol 2019**; 30(6). https://doi.org/10.1515/jbcpp-2019-0251.

41. Matondo A, Kilembe JT, Ngoyi EM, et al. Oleanolic acid, ursolic acid and apigenin from ocimum basilicum as potential inhibitors of the SARS-CoV-2 main protease: a molecular docking study. **Int J Pathog Res 2021**; 1: 1−16. https://doi.org/10.9734/ijpr/2021/v6i230156.
42. Hariyono P, Dwiastuti R, Yusuf M, Salin NH, Hariono M. 2-Phenoxyacetamide derivatives as SARS-CoV-2 main protease inhibitor: in silico studies. **Results Chem 2022**; 4:100263. https://doi.org/10.1016/j.rechem.2021.100263.
43. Rao Gajula SN, Pillai MS, Samanthula G, Sonti R. Cytochrome P450 enzymes: a review on drug metabolizing enzyme inhibition studies in drug discovery and development. **Bioanalysis 2021**; 13(17): 1355−1378. https://doi.org/10.4155/bio-2021-0132.

How to cite this article: Ibrahim ZY, Uzairu A, Shallangwa GA, Abechi SE, Isyaku S. Homology modeling, docking, and ADMET studies of benzoheterocyclic 4-aminoquinolines analogs as inhibitors of *Plasmodium falciparum*. J Taibah Univ Med Sc 2023;18(6):1200−1216.